ARTICLE   OPEN

Check for updates

Cross-hemispheric SST propagation enhances the predictability of tropical western Pacific climate

Cheng Sun [1]✉, Yusen Liu[1], Tian Wei[1], Fred Kucharski[2,3], Jianping Li [4,5] and Chunzai Wang [6]

The tropical western Pacific (TWP) has profound influences on climate. ENSO is an important source of interannual variability of TWP SST, but extratropical precursors are far less known. Here we show a significant interhemispheric influence from subtropical Southwest Pacific (SWP) on the TWP. Observational analysis suggests that SWP SST in boreal spring has strong coherence with TWP 6 months later. The spring SWP warming signal exhibits a unique interhemispheric propagation embedded in the southerly cross-equatorial flow over the western Pacific. The wind-evaporation-SST feedback initiates and maintains the progression of warm SST anomalies toward the TWP in autumn. The climate model successfully reproduces such an interhemispheric SST propagation. The seasonal evolution of SST variability improves the predictability of the warm pool SST by about 6 months. An SWP SST-based prediction model shows considerable hindcast skill ($r = 0.80$, $p < 0.01$), indicating that it is a valuable precursor of the TWP.

INTRODUCTION

The tropical western Pacific (TWP), where the world's largest warm pool is located, is characterized by the warmest sea waters among the tropical oceans, with the annual sea surface temperature (SST) exceeding 28 °C[1]. The TWP has dramatic impacts on the world's weather and climate[2–4]. The TWP is an essential source of kinetic energy and water vapor[5,6], driving large-scale atmospheric circulations and affecting precipitations locally and remotely[7,8]. Considering the large heat content and high SST in the TWP, it can easily trigger strong and deep convections. Consequently, it heats the upper-level troposphere[9] and transports water masses and energies toward the eastern Pacific and higher latitudes through both the Walker and Hadley circulations[5,10]. In addition to the local convective precipitation, the TWP can affect the monsoonal rainfall in East Asia via atmospheric teleconnection[11,12]. It also profoundly influences the numbers, genesis frequency, and tracks of tropical cyclones in the western North Pacific[13–15]. A previous study suggested that the size and intensity of the warm pool have undergone significant increases under the human-caused global warming[16]. It is almost certain that the impacts of the TWP on the global climate will increase substantially in the future. Therefore, it is of importance to understand the driving mechanisms and improve the prediction skills of the TWP SST variability by searching useful precursors.

The TWP is influenced by the convergence of tropical ocean currents driven by trade winds, local air-sea feedbacks (e.g., cirrus cloud; evaporation; convection), and large-scale atmospheric circulations[17–19]. The TWP warm SST episodes occur with a preference for spring and fall[7] when the maximum solar radiation reaches the tropics[20]. The seasonal variations of the TWP SST also result from the net surface heat fluxes associated with trade and monsoonal winds and horizontal/vertical oceanic advection[21]. On the interannual time scale, the TWP is an essential counterpart of the El Niño-Southern Oscillation (ENSO)

cycle. The migration of the warm pool (including centroid, east edge, and size) associated with surface winds and zonal oceanic advection is in phase with the ENSO variation[22,23]. In addition, heat content in the TWP also influences the intensity of the following ENSO[24]. Previous studies have demonstrated that the TWP SST and ENSO are closely correlated when ENSO leads by 5 months and the coverage of the warm pool expands eastward after the preceding ENSO[20]. Moreover, the ENSO-induced westward propagation of Rossby waves can influence the TWP SST variation and deep convection activities[25]. As suggested in the previous study, the close relationship between the TWP and ENSO enriched our understanding of the tropical ocean-atmosphere interactions and using the TWP as a precursor greatly improved the prediction skills of ENSO[22]. However, as most previous and current studies focus on the eastern Pacific SST variability predictions, the model performances in reproducing and predicting the TWP SST variability are far from skillful[26]. There is an urgent need to improve the predictability of the warm pool considering its dramatic impacts on the climate system, but finding useful precursors still remains an unresolved issue in the current literature.

Recent studies have highlighted a significant leading influence of extratropical variability on the tropical climate through air-sea interactions, particularly over the Northeast Pacific[27–30]. The propagations of extratropical SST anomalies to the tropics have been found in both hemispheres associated with the North/South Pacific meridional mode (NPMM/SPMM)[31,32], which has great implications for extending the predictability of the tropical eastern/central Pacific SSTs in terms of the time lags during the evolution[33,34]. In contrast, it is lesser-known in the literature whether there exist precursors or remote connections to the TWP SST outside the tropics. On the other hand, the SST in the Southwest Pacific (SWP) Ocean, south of the TWP, also exhibits significant interannual variability. Previous studies have suggested that the SWP SST is modulated by wind-driven air-sea heat

---

[1]College of Global Change and Earth System Science (GCESS), Beijing Normal University, Beijing, China. [2]The Abdus Salam International Centre for Theoretical Physics, Trieste, Italy. [3]Center of Excellence for Climate Change Research/Department of Meteorology, King Abdulaziz University, Jeddah, Saudi Arabia. [4]Frontiers Science Center for Deep Ocean Multispheres and Earth System (FDOMES)/Key Laboratory of Physical Oceanography/Academy of the Future Ocean, Ocean University of China, 266100 Qingdao, China. [5]Laboratory for Ocean Dynamics and Climate, Pilot Qingdao National Laboratory for Marine Science and Technology, 266237 Qingdao, China. [6]State Key Laboratory of Tropical Oceanography (LTO), South China Sea Institute of Oceanology, Chinese Academy of Sciences, Guangzhou, China. ✉email: scheng@bnu.edu.cn
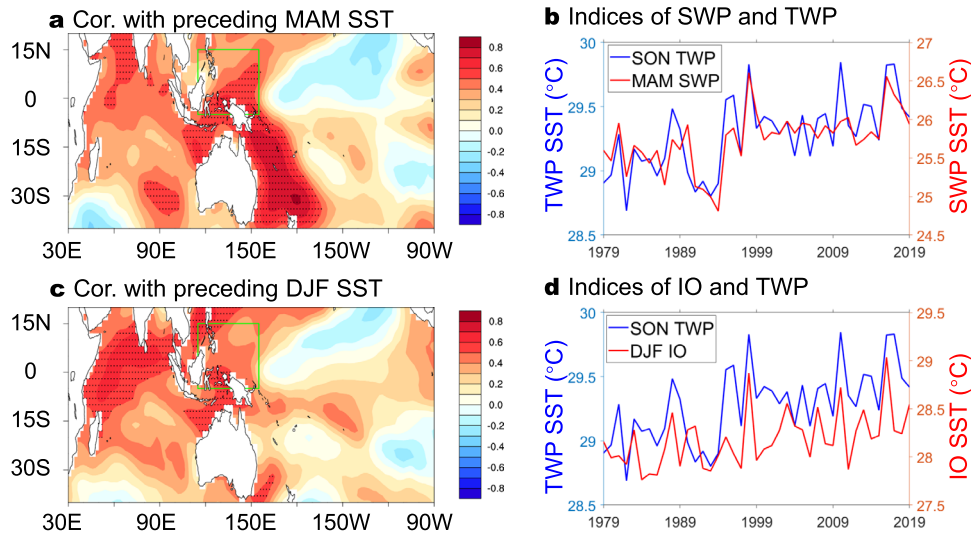
Fig. 1 Lead-lag relationship between the TWP and SWP. The correlations of the SON TWP (green box in the figure, 5°S–15°N, 115°E–155°E) SST index with the preceding (**a**) MAM and (**c**) DJF SST. **b** and **d** are the corresponding time series of Southwest Pacific SST index and Indian Ocean SST index for the period 1979–2019. They are defined as the weighted average of SSTs in the regions of (35°S–15°S, 150°E–170°E) and (5°S–10°N, 50°E–90°E), respectively. The dotted shading indicates the correlation is significant at the 95% confidence level.

fluxes[35], Ekman transport[36], and the subtropical western boundary currents[37], as well as ENSO[38]. The relationship between the SWP SST and the TWP SST is unclear. It is interesting to investigate if an extratropical-tropical teleconnection could be found in the western Pacific and the seasonally evolved SST anomalies may have great implications for improving the predicting skill of the TWP SST variability.

RESULTS

The interhemispheric connection between the SWP and TWP

The Maritime Continent (MC) lies in the heart of the western Pacific warm pool (TWP, 5°S–15°N, 115°–160°E), which is one of the largest heat and moisture sources of the global climate. During the boreal autumn (SON), the accumulated energy from the imported solar radiation makes surface/subsurface water the warmest in a year. As shown in Supplementary Fig. 1a, the highest SST is located in the northern sector of the TWP, while relatively cooler water is found in the tropical central Pacific. Previous studies suggest that the TWP is a so-called "rain pool" because the warm SSTs are strongly coupled with local precipitation[39]. The correlation maps of the TWP SST index with the tropical SST and MC rainfall are well corresponded. Moreover, the time series of TWP SST and precipitation indices are also in good agreement ($r = 0.67$), shown in Supplementary Fig. 2a. The warmer SST in the MC region increases the instability of the troposphere and feeds strong and deep convection to develop, resulting in more precipitation. Meanwhile, in the central Pacific, the subsidence corresponded with the strong ascending motions in the western Pacific prohibits local convection, resulting in less precipitation. Such contrasting rainfall distributions profoundly influence the imported fresh water and contribute to the formation of the salinity front in the central Pacific, which is related to ENSO[23]. Therefore, it is important to seek useful precursors of the autumn SST in the TWP, which not only helps the mitigations of severe floods in the populated MC region but also has implications for ENSO.

Through lead-lag correlations of the boreal autumn TWP SST index with global SSTs in preceding seasons, the SST warming signals are found most prominent in the SWP (SWP, 35°S–15°S, 150°E–170°E) during the boreal spring. As shown in Fig. 1a, warm waters are centered in the subtropical SWP Ocean and extend

toward the tropics along the east coast of Australia, exhibiting significant coherence with the following TWP SST ($r > 0.7$). We then compute the SWP SST index and compare it with the TWP SST index (Fig. 1b). The correlation coefficient between the two series reaches 0.80, with the SWP SST leading by two seasons, and the relationship is still prominent after removing the long-term trends ($r = 0.71$). The interannual variabilities of SST in these two regions are overall consistent for the period 1979–2019, and the years of maxima/minima generally correspond. During the analyzed period, the TWP SST has experienced a decadal shift around 1997/1998, which is consistently found in the SWP region. Based on the above temporal and spatial correlations, we may conclude that the autumn SST in the TWP region is closely connected with the preceding SST in SWP. The time lag between them may help improve the TWP SST predictability.

Previous studies suggest that the TWP SST is also associated with ENSO on the interannual time scale[23]. Therefore, the interannual variabilities between the MAM western Pacific SST and El Niño are carefully inspected by overlaying the two time series (supplementary Fig. 2b). The relationship between ENSO and TWP SST remains a lot of uncertainties ($r = 0.15$). The strong El Niño events simply do not promise a warmer TWP SST and the two time series barely agree in most La Nina years. In 1983 and 1992, the El Niño events corresponded with cooler SST in TWP, while the El Niño events in 1998, 2010, and 2016 corresponded with the following season TWP warming. The impact of ENSO on TWP SST cannot be ignored, but the robustness of their connections may raise further doubts. More importantly, the correlation coefficient between the SWP and TWP SST is still prominent after removing the preceding winter ENSO signal ($r = 0.80$), further suggesting that the SWP-TWP connection is statistically independent of ENSO.

We examine the correlation map of the TWP SST with the preceding winter (DJF) SSTs. In Fig. 1c, the eastern Pacific SST shows a weak and insignificant correlation. The most substantial warming is located in the Indian Ocean (IO). The correlation coefficient of the TWP SST with the DJF IO SST reaches 0.64 ($r = 0.50$ with detrended data), which is smaller than that with the MAM SWP SST, but the influence of the IO SST should not be neglected. Interestingly, the warming peaks of IO SST and TWP SST usually correspond to when strong El Niño events occurred in the winter (Fig. 1d). It is suggested that the ENSO signal can be
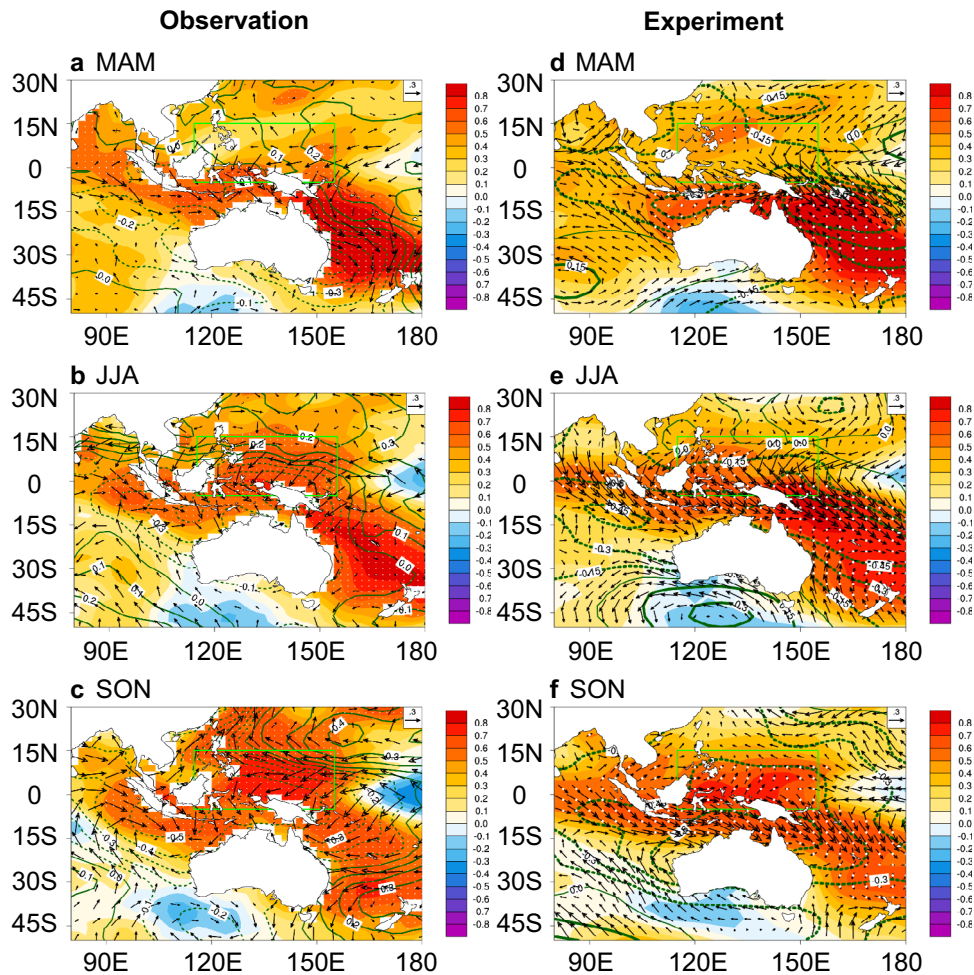
Fig. 2 Interhemispheric propagation of SST variability. The correlations maps of the MAM SWP SST index with the observed SST (shading), sea level pressure (contour) and winds (vector) in the **a** MAM, **b** JJA, **c** SON seasons for the period 1979–2019. **d**–**f** are for the simulation results of SWP_EXP pacemaker experiment (see Methods for details). The white dotted shading indicates the correlation is significant at the 95% confidence level.

anchored into the tropical IO via atmospheric teleconnection[40]. This may induce the following TWP warming due to an anomalous anticyclone and weakened cross-equatorial winds during the boreal summer and autumn. The footprint of the preceding ENSO signal may be embedded in the tropical IO and contributes, more or less, to the TWP warming in the following seasons. Nevertheless, we must note that the correlation between the TWP and SWP SST remains significant ($r = 0.69$), even when the preceding IO SST signal is removed. Thus, the SWP-TWP connection is unlikely dominated by either the DJF ENSO or IO SST. Such an independent relationship is robust during the analyzed period, and the underlying mechanisms require further investigation.

Interhemispheric propagation of SST variability

To understand how the TWP SST and SWP SST are connected, we calculate the lagged regressions of the SWP SST in the following seasons. In MAM (Fig. 2a), the SWP SST exhibits prominent warming, accompanied by an anomalous low. The warm water heats the lower-level troposphere and induces anomalous ascending motions, corresponding to pressure decline and large-scale convergence. Meanwhile, the warm water also extends toward the tropics in response to the subtropical SWP SST warming. Strong northwesterly winds converge to the low-pressure and further weaken the predominating southeast trade winds in the Southern Hemisphere tropics. The weakened wind

stress prohibits latent heat release, which leads to SST warming in the north of the low-pressure in the SWP region. This process agrees with the "wind-evaporation-SST" (WES) feedback[41], which has been suggested most effective in the tropical region. The tropical and subtropical sectors of SWP SST warming induce strong wind convergence in MAM, consequently resulting in an equatorward propagation of the SST warming signal and the corresponded low-pressure.

In JJA (Fig. 2b), as the anomalous SST warming reach the equator, the corresponding low-pressure and large-scale convergence induces strong cross-equatorial northerlies over the TWP, where southerlies dominate the climatological winds. The significant SST warming near the equator strengthens the anomalous northerly winds, which substantially reduces the southerly cross-equatorial flow over the Australia-Asia Monsoon region. As a result, the warm SST anomaly develops toward the western Pacific in the Northern Hemisphere. In SON (Fig. 2c), as the TWP SST continues to warm up, the main body of the warm anomaly moves across the equator and reaches its maximum intensity. Due to strong SST warming in the warm pool region, the atmospheric circulation exhibits a clear Gill-type response[42], with anomalous easterlies and a low-pressure center located in the tropics. Based on the above analysis, we may conclude that the preceding SST warming signal in the subtropical SWP indeed contributes to the development of the TWP. The seasonal evolving SST variability exhibits an interhemispheric propagation, which is likely dominated by the
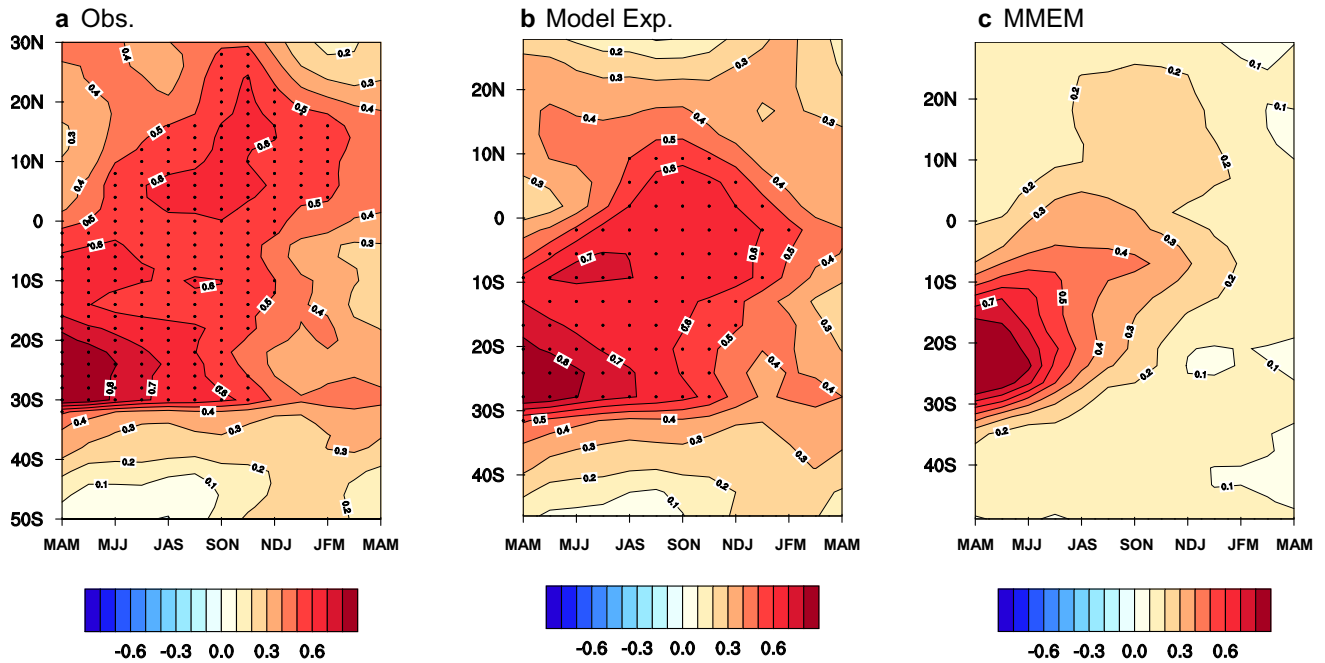
Fig. 3 Meridional evolution of SWP SST signal. The propagation of SWP SST signal indicated by the lagged correlations of the MAM SWP index with zonally averaged SST (115°E–160°E) in the following consecutive-3 months. **a** is the observation, **b** and **c** are for pacemaker experiment and SOM multi-model ensemble mean, respectively. The dotted shading in **a** and **b** indicates the correlation is significant at the 95% confidence level.

anomalous surface heat fluxes associated with weakened cross-equatorial winds.

To inspect the seasonal interhemispheric propagation of the SST warming signal from the SWP to the TWP, we calculated correlation coefficients of zonally averaged SST anomalies with the SWP SST index over consecutive-3 months. As shown in Fig. 3a, the largest correlations distribute in the Southern Hemisphere subtropics, corresponding to the SWP SST warming. In the following months, the SST warming signal propagates northward and crosses the equator during the boreal summer, and finally enters the Northwest Pacific, with strong SST warming in SON. The propagation process is consistent with the spatial regression in Fig. 2, verifying the influence of SWP SST on the following development of the TWP. More importantly, such an interhemispheric propagation of SST variability not only has implication for predicting the TWP SST variation but also indicate an approach of interhemispheric energy transmission.

As mentioned above, the cross-equatorial northerlies are essential for the SST signal to develop via suppressing the latent heat release in the underlying ocean. We further carry out net surface heat flux analysis by regressing the total and turbulent flux onto the SWP SST index during the boreal spring and summer. In MAM, the total net flux anomalies in the Southern Hemisphere favor ocean warming (supplementary Fig. 3a). As shown in Fig. 2a, the southern sector of the TWP is dominated by anomalous northwesterly winds related to the low pressure in SWP. The weakened southeast trade winds and prohibited latent heat release are reflected by decreased turbulent heat fluxes (supplementary Fig. 3c), close to the total flux pattern. In JJA, convergence toward the SST warming in subtropical SWP corresponds with strong cross-equatorial northerlies. As consistently shown in supplementary Fig. 3b and d, the reduced turbulent heat fluxes stride the equator and expand to the entire TWP region, resulting in SST warming. The extratropical-tropical propagation of SWP SST warming signal in the two Hemispheres is likely associated with the wind-driven thermodynamic process. Previous studies have suggested a southward progression

of SST anomalies over the North Pacific northeasterly trade region and the importance of mean flow in the SST propagations[30,43]. This study highlights the role of the southerly cross-equatorial monsoon in the propagation of SST variability over the western Pacific.

Model simulations

A partially coupled experiment isolating the effect of SWP SST (SWP_EXP, see Methods for details) is conducted to verify the connection between the SWP and TWP SST variabilities as well as the interhemispheric propagation. In MAM (Fig. 2d), the most prominent warming signal is found in the subtropical SWP with an extension toward the southern edge of TWP. During summer (Fig. 2e), the core of SST warming has moved into the tropical region and reached close to the equator. In contrast, the warming response in the northern sector of the warm pool is comparably weak and insignificant. In SON (Fig. 2f), the anomalous warm water has moved across the equator and covered the entire warm pool region. The Northern Hemisphere tropics exhibit strong warming in response to the preceding SWP SST signal, further verifying the lagged relationship between the SWP and TWP variabilities. In Fig. 3b, the simulated SST anomalies exhibit consistent meridional propagations from MAM to SON, consistent with the observation. The subtropical SWP SST warming signal propagates northward and moves across the equator into the Northern Hemisphere. The northern edge of the SST anomaly reaches 20°N in model simulation, while it can even extend beyond the tropic in observations. The influence of the background warming trend on the simulation of the cross-season SST coherence is also investigated. With the background warming trend removed, we examine the simulated lagged correlations between the MAM SWP index and SON SST in the SWP_EXP as shown in Supplementary Fig. 6. The lagged response of TWP SST to the MAM SWP SST forcing and the cross-season SST coherence remain significant.

The propagation of the SWP SST is also inspected in an ensemble of five slab ocean models (see Methods for details).

As shown in Fig. 3c, the ensemble mean also indicates a seasonal propagating feature of the SWP SST anomaly. However, there is a significant underestimation of the SST warming in the Northern Hemisphere since JJA, which is probably due to that the response is canceled out through ensemble mean. We examine the simulated evolution in each model. Most of the models exhibit lagged responses of significant SST warming in the Northern Hemisphere tropics. As shown in Supplementary Fig. 4, the five models successfully reproduce the seasonal northward propagation that somewhat resembles the observation, further indicating that the connection between the SWP and TWP is robust. Based on the above analysis, it is clearly shown in both observation and pacemaker experiment that an interhemispheric propagation bridges the subtropical SST anomaly in the Southern Hemisphere and the TWP warm pool in the Northern Hemisphere.

To understand the mechanism behind the SST propagation, the corresponding wind and heat fluxes in the slab ocean model simulation are analyzed. As shown in Fig. 2d, the strong SST warming induces a low-pressure in the SWP and the corresponded convergence from the tropics in MAM, consistent with the observation. The converged northwesterly is mainly confined to the tropical region, where it is the northern edge of the subtropical heat source. During the boreal spring, the southeast trade wind prevails in climatology, whereas, in this case, the SWP SST warming-induced northerly convergence enhances, resulting in significantly reduced surface wind stress in the Southern Hemisphere tropics. Consequently, surface evaporation is prohibited, which leads to a decrease in surface turbulent heat flux (supplementary Fig. 5c). The reduced turbulent heat flux agrees with the changes in total heat flux (supplementary Fig. 5a), which is confined to the Southern Hemisphere and significantly contributes to SST warming. Thus, the tropical SST warming could be finely explained by the weakened trade winds, consistent with the observation. As the SST warming signal extends toward the tropics from the subtropical SWP due to reduced turbulent heat flux, strong northerly wind constantly converges to the northern edge of the warming region. In JJA (Fig. 2e), the warm water centers in the tropics and steadily approaches the southern side of the equator. Accordingly, the converged wind belt moves northward, exhibiting strong cross-equatorial wind from the Northern Hemisphere tropics, which is exactly the opposite direction of the predominate southerly in climatology. The weakened cross-equatorial winds decrease the turbulent heat flux as in MAM. As shown in supplementary Fig. 5d, the turbulent heat flux has moved across the equator and dominates in the Northern

Hemisphere, resulting in the cross-equatorial SST anomaly during summer. Both the total (supplementary Fig. 5b) and turbulent flux exhibit a consistent arch-shaped pattern, which is well corresponded with the wind anomalies and surface SST warming. The above analysis indicates that the meridional SST propagation is main driven by turbulent heat flux anomaly associated with cross-equatorial winds. In SON (Fig. 2f), the SST warming is most prominent in the warm pool region (north of the equator), accompanied by a Gill-type response. In this case, the simulated atmospheric circulation is more likely a response to the underlying ocean warming than a forcing, consistent with the observation. For the pacemaker experiment based on the slab ocean model, SSTs outside the prescribed region only respond to the local air-sea interactions forced by the "pacemaker" and the associated atmospheric circulation anomalies. In this study, the slab ocean model is able to reproduce the observed SST propagation as well as the wind and surface heat flux anomalies, further highlighting a vital role of thermodynamics in the interhemispheric propagation of SST variabilities.

A prediction model of the TWP

Based on the above analysis, we find strong coherence between the SWP SST variability and the TWP, which is robust in both observation and model simulations. The interhemispheric propagation of SST variability produces lagged response for about two seasons, which makes the MAM SST in the subtropical SWP a potential precursor of the warm pool during the boreal summer. The physical mechanism for interhemispheric propagation is summarized in Fig. 4. The inter-seasonal northward progression of SST anomalies from the SWP to TWP is concurrent with the northward migration of the Intertropical Convergence Zone (ITCZ) and the seasonal development of cross-equatorial southerly flow (Supplementary Fig. 8). The coupled interaction between changes in the surface winds and SST plays a key role in initializing and maintaining the SST progressions.

As shown in Fig. 1c, the DJF IO SST also leads and contributes to the following TWP warming to some extent. Despite that the preceding warming signal in the IO is weaker than that in the SWP, the IO SST, more or less, contains the influence of ENSO and shows correspondence with the TWP during some peak years[40]. Previous studies have shown that the warm SST anomaly in the tropical IO has a strong persistence from the boreal winter to the following summer, and the internal ocean–atmosphere interaction within the basin is the key to maintaining the SST warming signal through winter and spring[40,44]. The persistent IO SST warming
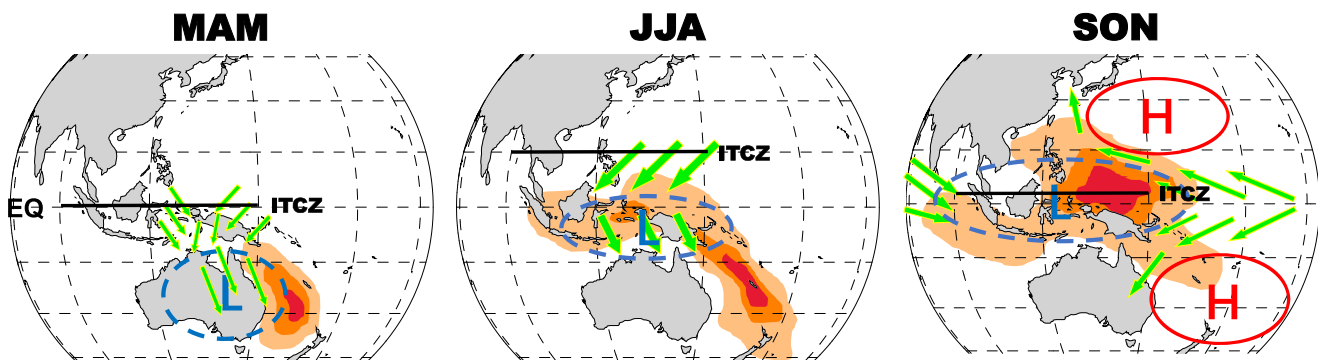

Fig. 4 Schematic of mechanisms. Schematic summarizing the interhemispheric propagation of western Pacific SST anomalies starting from boreal spring as described in this study. Green arrows are surface wind anomalies. Solid black line is the approximate position of the western Pacific ITCZ in different seasons. Dashed and solid circles represent anomalous low and high pressure, respectively. Colored shading denotes SST anomalies. During boreal spring, the SWP warming-induced anomalous low pressure and northerly winds weaken the trade winds south of the equator, initiating the WES feedback. During boreal summer, the SST warming progresses toward the north of Australia, and the atmospheric responses lead to modulation of cross-equatorial monsoon flow and suppression of turbulent flux release in tropical western Pacific. The WES feedback maintains the northward propagation of SST anomalies. During boreal autumn, the warming signal crosses the equator into the northern western Pacific, influencing the Northern Hemisphere climate.

further induces a Gill-type response in summer, with low-pressure anomalies over the IO and an anomalous high located to the east of the IO heating (Supplementary Fig. 9). The anomalous surface high over the northwestern tropical Pacific in response to the IO warming is consistent with the previous findings[40,45]. This high-pressure anomaly is accompanied by divergent flow and north-easterly winds near the equator (Supplementary Fig. 9), contributing to the reduction of southerly monsoon flow in summer and the suppression of latent heat release in the underlying ocean. This mechanism may explain the connections between the winter IO SST and the TWP SST in the following seasons. It is different from the cross-hemispheric influence of the SWP SST, which highlights the inter-seasonal northward SST propagation from the SWP to TWP and the coupled interactions between the atmosphere and the SST across the western Pacific.

Thus, a TWP variability prediction model is constructed based on the preceding MAM SWP SST and DJF IO SST for the period 1979–2019 [Eq. 1]:

$$TWP_{SON} = a * SWP_{MAM} + b * IO_{DJF} + c \tag{1}$$

where a, b, and c are coefficients. The prediction model is examined using a ten-fold cross-validation method. The correlation coefficients of the hindcast results in the cross-validation with the observed series is high ($r = 0.80$, $p < 0.01$), further indicating a rather skillful prediction for the TWP SST variability, which is more skillful than using either the SWP ($r = 0.76$) or IO ($r = 0.60$) separately. The modeled series generally captures those warming peaks in the TWP, and corresponds well with the observation in recent years (Fig. 5). The SWP SST-based model further verifies the teleconnection between the SWP and TWP, introducing a new extratropical precursor to the warm pool. It could improve the predictability of the TWP SST variability as well as the TWP precipitation, which shows close associations with the underlying SST.

DISCUSSION

During the boreal autumn, the western Pacific warm pool reaches its maximum intensity and profoundly influences convective rainfalls over the MC, threatening human lives and causing considerable economic losses. We find strong coherence between SST and precipitation on the interannual time scale, thus improving the predictability of warm pool SST is of importance to mitigate and prevent losses from heavy rainfall and floods. This study finds significant correlations between the subtropical SWP and TWP with a time lag of two seasons. The SWP warming signal progresses toward the TWP in the southerly monsoon region from boreal spring to autumn. Northerly anomalies induced by the SWP warming weaken the mean flow and initiate the northward propagation of SST warming through the WES feedback. A SWP pacemaker experiment and an ensemble of five slab ocean models successfully reproduced the above processes, further indicating the robust connection between the SWP and TWP SST variabilities. Considering the lagged response of TWP to the preceding SWP SST signal, a prediction model is constructed and

verified using the ten-fold cross-validation method. The hindcast results are in good correspondence with the observed series ($r = 0.80$), exhibiting considerable predicting skill of the TWP SST variability. This finding not only indicates a precursor of the TWP from the Southern Hemispheric extratropics, more importantly, it indicates a pattern of interhemispheric propagation of SST variability and energy transmission between the two hemispheres, which is embedded in the southerly cross-equatorial flow over the Asian-Australia monsoon region and mainly driven by the wind-related thermodynamic processes.

As suggested in previous studies[22,23], the variability of TWP is closely related to the ENSO cycle. In this study, the relationship between the SON TWP and the preceding DJF ENSO is weak ($r = 0.15$). The relationship between the SWP and TWP is still prominent even after removing the preceding winter ENSO signal ($r = 0.80$), indicating that the SWP-TWP teleconnection is unlikely dominated by ENSO. Previous studies have shown that a developing ENSO could have instantaneous impacts on western Pacific SST before the matured phase[46], and the instantaneous correlations between ENSO signal and Pacific SST in different seasons indeed show modest correlations in the western Pacific (Supplementary Fig. 7a–c). However, the cross-season influence of SWP SST on the TWP is independent of the developing phase of ENSO, and the cross-season coherence remains strong with the seasonal ENSO signal removed (Supplementary Fig. 7d–e). The influence of ENSO may be anchored in the IO "capacitor," which delivers lagged response to the TWP during some peak years. Thus, the DJF IO SST signal is also included in the prediction model to better depict the warm pool variability.

In this study, only the slab ocean model is used, and it reasonably well reproduces the propagating characteristics and the associated heat flux anomalies, indicating an important role of thermodynamics. Previous studies have also suggested that the SST warming associated with the prohibited latent heat release is mainly modulated by the reduced surface winds in the TWP, where the climatological SST is high[47,48]. Nevertheless, there are some differences between the model simulation (SWP_EXP) and the observation, such as the location of SST warming centers during the course of the northward propagations, and such a bias is likely associated with the lack of ocean dynamic process in the slab ocean model simulation. The ocean dynamic processes, such as the Australian western boundary current and tropical zonal currents, may deepen our understanding of the interhemispheric propagation of western Pacific SST variability and its relation with ENSO and should be considered in future works.

METHODS

Data

In this study, the precipitation data is derived from the Global Precipitation Climatology Project (GPCP) Monthly Precipitation Analysis (available at https://psl.noaa.gov/data/gridded/data.gpcp.html)[49]. The sea surface temperature data is derived from Extended Reconstructed SST version 5 (available at https://psl.noaa.gov/data/gridded/data.noaa.ersst.v5.html)[50]. The atmospheric data for sea level pressure, surface winds are derived from the ECMWF reanalysis, ERA5[51]. Compared with the previous versions, the ERA5 product shows a significant improvement in representing the variability and magnitude of near-surface air temperature and wind fields. The surface heat flux data are also derived from the ERA5 product, and the net surface heat flux is defined to be positive downward in this study. All data are employed and analyzed for the period 1979–2019.

Experimental design

The SWP pacemaker experiment (a partially coupled simulation isolating the effect of SWP SST, referred to as SWP_EXP) is conducted using the International Centre for Theoretical Physics (ICTP) AGCM version 41[52] coupled to a slab ocean mixed-layer model (SOM). The ICTPAGCM is an intermediate complexity model that contains eight vertical levels with a horizontal resolution of T30 (3.75° × 3.75° grid). The SWP_EXP experiment
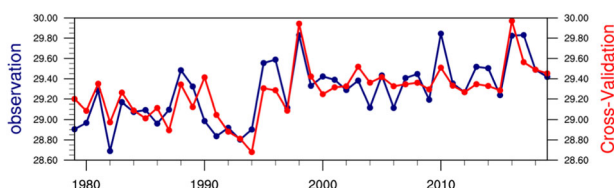
Fig. 5 Hindcast of the SWP SST-based prediction model. The observed (blue) and hindcasted (red) SST series (units: °C) of the TWP using the ten-fold cross-validation method (see Methods for details) for the period 1979–2019.

aims to examine the atmospheric and SST responses to SWP warming outside the SWP region and associated atmosphere-ocean interactions at seasonal to interannual timescales. The raw observed monthly-varying SSTs are prescribed in the SWP Ocean (40°–10°S, 130°E–170°W) while the ICTPAGCM is run coupled to the slab ocean model outside the SWP region (see Supplementary Fig. 10 for the location of the decoupled area). The surface/subsurface ocean temperature is calculated based on the net heat flux into the ocean, which excludes the dynamic processes, such as ocean advection or entrainment. The model integrations start in 1950 and run through 2019. An ensemble of five members is generated by restarting the model using small initial perturbations. The first 29 years of all simulations are considered as spin-up and the analysis is performed on the remaining period from 1979–2019, consistent with the observations.

Besides the SWP_EXP, we also used simulation results from an ensemble of the AGCMs, coupled to a 50 m-deep slab-ocean mixed-layer model (hereafter referred to as slab-ocean models). This ensemble of slab ocean models is used to access the model dependence of the simulation results. These Slab-ocean simulations are run with constant preindustrial forcing and a prescribed annual cycle of ocean heat transport. Five models are used, and the simulation output data can be accessed through the Centre for Environmental Data Analysis (CEDA) archive (https://catalogue.ceda.ac.uk/). The five SOMs (simulation length in years) analyzed are as follows: MPIM-ECHAM5 (100), GFDL-CM2.1 (100), INM-CM3 (60), MRI-CGCM2-3-2 (150) and MIROC (60). Monthly mean fields from the model output are interpolated to the T42 grid, and the annual cycle is removed before calculating the seasonal mean anomalies.

Statistical analysis

In this study, a k-fold cross-validation method[53] is used to examine the capability of the SWP SST-based prediction model. The raw series is divided into ten groups (k = 10). In each run, one group is eliminated from the series while letting the remaining groups train the prediction model and examined by the eliminated one. The hindcast results are derived by averaging the ten repeatedly constructed series.

The statistical significance in the linear correlation of two autocorrelated series is examined by the two-tail Student's t test. The effective number of degrees of freedom[54,55] is calculated by [Eq. 2]:

$$\frac{1}{N^{eff}} \approx \frac{1}{N} + \frac{2}{N}\sum_{j=1}^{N}\frac{N-j}{N}\rho_{XX}(j)\rho_{YY}(j) \qquad (2)$$

where N represents the sample size, $\rho_{XX}(j)$ is for the autocorrelation of time series X and $\rho_{YY}(j)$ is for Y, here j is the time lag.

DATA AVAILABILITY

The original observational data are publicly available. All data sources are mentioned in the Methods section.

CODE AVAILABILITY

The source codes for the analysis of this study are available from the corresponding author upon reasonable request. The code of ICTPAGCM is available through the URL: https://www.ictp.it/research/esp/models/speedy.aspx.

REFERENCES

1. Webster, P. J. & Lukas, R. TOGA COARE: the coupled ocean–atmosphere response experiment. Bull. Am. Meteorol. Soc. **73**, 1377–1416 (1992).
2. Hoerling, M. & Kumar, A. The perfect ocean for drought. Science **299**, 691–694 (2003).
3. Palmer, T. & Mansfield, D. Response of two atmospheric general circulation models to sea-surface temperature anomalies in the tropical east and west Pacific. Nature **310**, 483–485 (1984).
4. Trenberth, K. E. et al. Progress during TOGA in understanding and modeling global teleconnections associated with tropical sea surface temperatures. J. Geophys. Res.: Oceans **103**, 14291–14324 (1998).
5. Graham, N. & Barnett, T. Sea surface temperature, surface wind divergence, and convection over tropical oceans. Science **238**, 657–659 (1987).
6. Sardeshmukh, P. D. & Hoskins, B. J. The generation of global rotational flow by steady idealized tropical divergence. J. Atmos. Sci. **45**, 1228–1251 (1988).
7. Fasullo, J. & Webster, P. J. Warm pool SST variability in relation to the surface energy balance. J. Clim. **12**, 1292–1305 (1999).
8. Neale, R. & Slingo, J. The Maritime Continent and its role in the global climate: A GCM study. J. Clim. **16**, 834–848 (2003).
9. Webster, P. J. The role of hydrological processes in ocean-atmosphere interactions. Rev. Geophys. **32**, 427–476 (1994).
10. Bjerknes, J. Atmospheric teleconnections from the equatorial Pacific. Monthly Weather Rev. **97**, 163–172 (1969).
11. Huang, R. & Sun, F. Impacts of the tropical western Pacific on the East Asian summer monsoon. J. Meteorol. Soc. Jpn. Ser. II **70**, 243–256 (1992).
12. Nitta, T. Convective activities in the tropical western Pacific and their impact on the Northern Hemisphere summer circulation. J. Meteorol. Soc. Jpn. Ser. II **65**, 373–390 (1987).
13. Wang, L. & Chen, G. Impact of the Spring SST Gradient between the Tropical Indian Ocean and Western Pacific on Landfalling Tropical Cyclone Frequency in China. Adv. Atmos. Sci. **35**, 682–688 (2018).
14. Webster, P. J., Holland, G. J., Curry, J. A. & Chang, H.-R. Changes in tropical cyclone number, duration, and intensity in a warming environment. Science **309**, 1844–1846 (2005).
15. Zhan, R., Wang, Y. & Wen, M. The SST gradient between the southwestern Pacific and the western Pacific warm pool: a new factor controlling the northwestern Pacific tropical cyclone genesis frequency. J. Clim. **26**, 2408–2415 (2013).
16. Weller, E. et al. Human-caused Indo-Pacific warm pool expansion. Sci. Adv. **2**, e1501719 (2016).
17. McPhaden, M. J. & Hayes, S. P. On the variability of winds, sea surface temperature, and surface layer heat content in the western equatorial Pacific. J. Geophys. Res.: Oceans **96**, 3331–3342 (1991).
18. Ramanathan, V. & Collins, W. Thermodynamic regulation of ocean warming by cirrus clouds deduced from observations of the 1987 El Nino. Nature **351**, 27–32 (1991).
19. Waliser, D. E. & Graham, N. E. Convective cloud systems and warm-pool sea surface temperatures: Coupled interactions and self-regulation. J. Geophys. Res.: Atmos. **98**, 12881–12893 (1993).
20. Kim, S. T., Yu, J. Y. & Lu, M. M. The distinct behaviors of Pacific and Indian Ocean warm pool properties on seasonal and interannual time scales. J. Geophys. Res.: Atmos. **117**, D05128 (2012).
21. Schneider, N., Barnett, T., Latif, M. & Stockdale, T. Warm pool physics in a coupled GCM. J. Clim. **9**, 219–239 (1996).
22. Clarke, A. J. & Van Gorder, S. ENSO prediction using an ENSO trigger and a proxy for western equatorial Pacific warm pool movement. Geophys. Res. Lett. **28**, 579–582 (2001).
23. Picaut, J., Ioualalen, M., Menkès, C., Delcroix, T. & Mcphaden, M. J. Mechanism of the zonal displacements of the Pacific warm pool: Implications for ENSO. Science **274**, 1486–1489 (1996).
24. Sun, D.-Z. A possible effect of an increase in the warm-pool SST on the magnitude of El Niño warming. J. Clim. **16**, 185–205 (2003).
25. Chen, G. & Qin, H. Strong ocean–atmosphere interactions during a short-term hot event over the western Pacific warm pool in response to El Niño. J. Clim. **29**, 3841–3865 (2016).
26. Yang, Y., Wang, F. & Zheng, J. CMIP5 model biases in the climatological mean state of the western Pacific warm pool. Theor. Appl. Climatol. **140**, 533–545 (2020).
27. Chiang, J. C. & Vimont, D. J. Analogous Pacific and Atlantic meridional modes of tropical atmosphere–ocean variability. J. Clim. **17**, 4143–4158 (2004).
28. Li, J., Zheng, F., Sun, C., Feng, J. & Wang, J. Pathways of influence of the Northern Hemisphere mid-high latitudes on East Asian climate: A review. Adv. Atmos. Sci. **36**, 902–921 (2019).
29. Liu, Y. et al. The North Pacific Blob acts to increase the predictability of the Atlantic warm pool. Environ. Res. Lett. **16**, 064034 (2021).
30. Vimont, D. J., Battisti, D. S. & Hirst, A. C. Footprinting: A seasonal connection between the tropics and mid-latitudes. Geophys. Res. Lett. **28**, 3923–3926 (2001).
31. Chang, P. Pacific meridional mode and El Ni¤o-Southern oscillation. Geophys. Res. Lett. **34**, L16608 (2007).
32. Zhang, H., Clement, A. & Di Nezio, P. The South Pacific meridional mode: a mechanism for ENSO-like variability. J. Clim. **27**, 769–783 (2014).
33. Larson, S. & Kirtman, B. The Pacific Meridional Mode as a trigger for ENSO in a high-resolution coupled model. Geophys. Res. Lett. **40**, 3189–3194 (2013).
34. Liguori, G. & Di Lorenzo, E. Separating the North and South Pacific meridional modes contributions to ENSO and tropical decadal variability. Geophys. Res. Lett. **46**, 906–915 (2019).
35. Guan, Y., Zhu, J., Huang, B., Hu, Z.-Z. & Kinter, J. L. III South Pacific Ocean dipole: A predictable mode on multiseasonal time scales. J. Clim. **27**, 1648–1658 (2014).
36. Rintoul, S. R. & England, M. H. Ekman transport dominates local air–sea fluxes in driving variability of Subantarctic Mode Water. J. Phys. Oceanogr. **32**, 1308–1321 (2002).

37. Hill, K., Rintoul, S., Ridgway, K. & Oke, P. Decadal changes in the South Pacific western boundary current system revealed in observations and ocean state estimates. *J. Geophys. Res.: Oceans* **116**, C01009 (2011).

38. Greig, M. J., Ridgway, N. M. & Shakespeare, B. S. Sea surface temperature variations at coastal sites around New Zealand. *N.Z. J. Mar. Freshw. Res.* **22**, 391–400 (1988).

39. Chen, G., Fang, C., Zhang, C. & Chen, Y. Observing the coupling effect between warm pool and "rain pool" in the Pacific Ocean. *Remote Sens. Environ.* **91**, 153–159 (2004).

40. Xie, S.-P. et al. Indian Ocean capacitor effect on Indo–western Pacific climate during the summer following El Niño. *J. Clim.* **22**, 730–747 (2009).

41. Xie, S. P. A coupled ocean-atmosphere model of relevance to the ITCZ in the eastern Pacific. *Tellus A* **46**, 340–350 (1994). Philander SGH.

42. Gill, A. E. Some simple solutions for heat-induced tropical circulation. *Q. J. R. Meteorol. Soc.* **106**, 447–462 (1980).

43. Chiang, J. C. & Bitz, C. M. Influence of high latitude ice cover on the marine Intertropical Convergence Zone. *Clim. Dyn.* **25**, 477–496 (2005).

44. Du, Y., Xie, S. P., Huang, G. & Hu, K. M. Role of Air-Sea Interaction in the Long Persistence of El Nino-Induced North Indian Ocean Warming. *J. Clim.* **22**, 2023–2038 (2009).

45. Xie, S. P. et al. Indo-western Pacific ocean capacitor and coherent climate anomalies in post-ENSO summer: a review. *Adv. Atmos. Sci.* **33**, 411–432 (2016).

46. Kucharski, F. et al. A Gill-Matsuno-type mechanism explains the tropical Atlantic influence on African and Indian monsoon rainfall. *Q. J. R. Meteorological Soc.: A J. Atmos. Sci. Appl. Meteorol. Phys. Oceanogr.* **135**, 569–579 (2009).

47. Wu, R. G., Kirtman, B. P. & Pegion, K. Surface latent heat flux and its relationship with sea surface temperature in the National Centers for Environmental Prediction Climate Forecast System simulations and retrospective forecasts. *Geophys. Res. Lett.* **34**, L17712 (2007).

48. Zhang, G. J. & McPhaden, M. J. The relationship between sea-surface temperature and latent-heat flux in the equatorial Pacific. *J. Clim.* **8**, 589–605 (1995).

49. Adler, R. F. et al. The version-2 global precipitation climatology project (GPCP) monthly precipitation analysis (1979-present). *J. Hydrometeorol.* **4**, 1147–1167 (2003).

50. Huang, B. et al. Extended reconstructed sea surface temperature, version 5 (ERSSTv5): upgrades, validations, and intercomparisons. *J. Clim.* **30**, 8179–8205 (2017).

51. Hersbach, H. et al. The ERA5 global reanalysis. *Q. J. R. Meteorol. Soc.* **146**, 1999–2049 (2020).

52. Kucharski, F. et al. The teleconnection of the tropical Atlantic to Indo-Pacific sea surface temperatures on inter-annual to centennial time scales: a review of recent findings. *Atmosphere* **7**, 29 (2016).

53. Michaelsen, J. Cross-validation in statistical climate forecast models. *J. Appl. Meteorol. Climatol.* **26**, 1589–1600 (1987).

54. Li, J., Sun, C. & Jin, F. F. NAO implicated as a predictor of Northern Hemisphere mean temperature multidecadal variability. *Geophys. Res. Lett.* **40**, 5497–5502 (2013).

55. Pyper, B. J. & Peterman, R. M. Comparison of methods to account for auto-correlation in correlation analyses of fish data. *Can. J. Fish. Aquat. Sci.* **55**, 2127–2140 (1998).

AUTHOR CONTRIBUTIONS

C.S., designed the research. C.S., Y.L., and T.W. performed the data analysis, prepared all figures and led the writing of the paper. All the authors discussed the results and commented on the paper.

COMPETING INTERESTS

The authors declare no competing interests.

ADDITIONAL INFORMATION

Supplementary information The online version contains supplementary material available at https://doi.org/10.1038/s41612-022-00262-6.

Correspondence and requests for materials should be addressed to Cheng Sun.

Reprints and permission information is available at http://www.nature.com/reprints

Publisher's note Springer Nature remains neutral with regard to jurisdictional claims in published maps and institutional affiliations.